Journal of Nuclear Materials 393 (2009) 333–342

Contents lists available at ScienceDirect

Journal of Nuclear Materials

journal homepage: www.elsevier.com/locate/jnucmat

Review

Thermodynamic and experimental study of UC powders ignition

F. Le Guyadec [a,*], C. Rado [a], S. Joffre [a], S. Coullomb [a], C. Chatillon [b], E. Blanquet [b]

[a] Commissariat à l'Énergie Atomique CEA–MARCOULE, DEN/DTEC/SDTC/Laboratoire d'Etude des Matériaux en Environnement, BP 17171, 30207 Bagnols sur Cèze, France
[b] SIMAP, Sciences et Ingénierie des Matériaux et Procédés, INPG–CNRS–UJF ENSEEG, BP 75, 38402 St Martin-d'Hères, France

ARTICLE INFO

Article history:
Received 20 January 2009
Accepted 8 June 2009

ABSTRACT

Mixed plutonium and uranium carbide (UPuC) is considered as a possible fuel material for future nuclear reactors. However, UPuC is pyrophoric and fine powders of UPuC are subject to temperature increase due to oxidation with air and possible ignition during conditioning and handling. In a first approach and to allow easier experimental conditions, this study was undertaken on uranium monocarbide (UC) with the aim to determine safe handling conditions for the production and reprocessing of uranium carbide fuels. The reactivity of uranium monocarbide in oxidizing atmosphere was studied in order to analyze the ignition process. Experimental thermogravimetric analysis (TGA) and differential thermal analysis (DTA) revealed that UC powder obtained by arc melting and milling is highly reactive in air at about 200 °C. The phases formed at the various observed stages of the oxidation process were analyzed by X-ray diffraction. At the same time, ignition was analyzed thermodynamically along isothermal sections of the U-C-O ternary diagram and the pressure of the gas produced by the UC + O_2 reaction was calculated. Two possible oxidation schemes were identified on the U-C-O phase diagram and assumptions are proposed concerning the overall oxidation and ignition paths. It is particularly important to understand the mechanisms involved since temperatures as high as 2500 °C could be reached, leading to CO(g) production and possibly to a blast effect.

Contents

1. Introduction

Uranium monocarbide (UC) is a possible fuel for nuclear reactors of the 4th-generation [1]. Published autoignition temperatures and oxidation mechanisms for this compound vary widely depending in particular on the powder processing, the powder specific surface, the processing atmosphere [2–4] and partial pressures. The risk of pyrophoricity, and thus of a sudden temperature rise for fine powders [5,6] is much greater than for the bulk compound. Ignition temperatures ranging from room temperature to 300 °C have been reported, depending mainly on the materials morphology. The present oxidation study deals with materials elaborated under known and controlled conditions, and characterized after processing. Our objective is to define a test methodology to assess their pyrophoricity and determine safe handling conditions reliable for fuel elaboration, reprocessing and storage.

2. Experimental equipment and UC materials

Uranium monocarbide (UC) was produced by arc melting of solid uranium and carbon as a pod weighing about 1 g which was then ground for 5 h in dodecane to prevent oxidation. The laser particle size measurement data are summarized in Table 1.

* Corresponding author. Tel.: +33 04 66 33 93 12; fax: +33 04 66 79 66 25.
E-mail address: fabienne.leguyadec@cea.fr (F. Le Guyadec).

0022-3115/$ - see front matter © 2009 Elsevier B.V. All rights reserved.
doi:10.1016/j.jnucmat.2009.06.009

Table 1
UC particle size distribution after 5 h milling time (D_x means that x% of the powder has a diameter below the indicated value).

Milling time	D_{50} (μm)	D_{10} (μm)	D_{90} (μm)
5 h	1.5	0.7	2.6

The powder was then stored in dodecane. Prior to DTA oxidation tests the UC powder was dried for 70 h at 50 °C in 6.0 Ar flow. The characterization of the dried powder (XRD, SEM on polished cross-sections) showed that the sample was not oxidized i.e. no oxide layer was observed at the micrometric scale which does not discard any native thin oxide layer (usually about 1–2 nm).

Oxidation tests were performed in a Setaram TGA92 DTA/TGA thermobalance, fitted with alumina internal structures (DTA probe and laboratory tube). The device operates with flowing air or various other gases. Differential thermal analysis (DTA) is a measure of the temperature difference versus time or temperature between the sample and a reference, when subjected to programmed temperature ramps under controlled atmosphere flow.

The wet mass (UC + dodecane) used for the DTA tests was between 75 and 100 mg, corresponding to about 50–70 mg of dried UC powder. The wet sample loaded in a cylindrical alumina crucible was placed in the thermobalance, heated at 50 °C under Ar flow for drying and then submitted to an adjustable programmed heating ramp up to 500 °C in controlled dry air flow. Using TGA simultaneously, the sample weight gain was also monitored. The ignition point was identified as the point of intersection of the tangents to the curves before and after excess heat exchange. At the end of the test, the oxidized powder was allowed to cool down to room temperature when switching to pure Ar flow, then collected in silicone grease for X-ray diffraction analysis.

3. Thermodynamic study

From literature data, the U-C-O system has been studied at high temperatures (1300–2300 °C) by phase analysis and gas pressure determinations (mainly oxygen and CO(g)). Recently, all the reported phases analysis and vapor pressure determinations (oxygen activities) were critically examined [7,8] to propose selected reliable thermodynamic and phase diagram data. Optimization was performed by Guéneau et al. [9] using the ThermoCalc software based on defects modelling for non-stoichiometric compounds:

- For U-C, a previous work [10] based on point defects in U–C compounds: UC, UC_2 and U_2C_3.
- For U–O, an optimization work with point defects for $UO_{2\pm x}$ [11] based on a critical assessment of experimental data [12–15].

Optimization results for the U–C–O system [9] were used in the present study and computations presented here were obtained using the ThermoCalc software. Two types of thermodynamic calculations were performed: isothermal cross-sections of the U-C-O ternary diagram calculated at 227 °C (Figs. 1–3) and gas pressures calculated for the triphasic domains concerned by the overall combustion phenomenon.

Our objective here is not to define *a priori* the UC oxidation path, but to describe phase diagram in the domain of compositions concerned by the oxidation i.e. along the line UC–½O_2 (see dashed line in Fig. 1).

Concerning the uranium carbides, Bessmann [16] observed that the formation of the sesquicarbide U_2C_3 is sluggish at temperatures about 800 °C meanwhile the UC_2 carbide is more quickly formed. So, we will probably observe either the U_2C_3 or UC_2 compound depending on the reaction rates during oxidation or ignition. In the phase diagram calculations, we chose to consider the stable U_2C_3 compound.

Furthermore, in our calculations, we assume that the solid solution $UC_{1-x}O_x$ exists from room temperature to high temperature

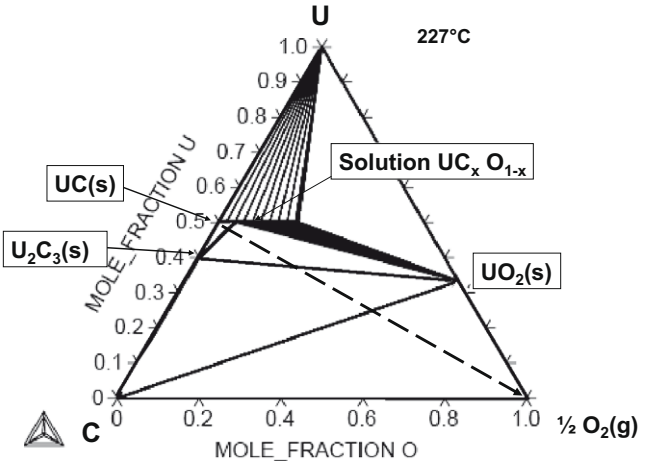

Fig. 1. Calculated isothermal cross-section of the U-C-O ternary phase diagram at 227 °C and 1 bar.

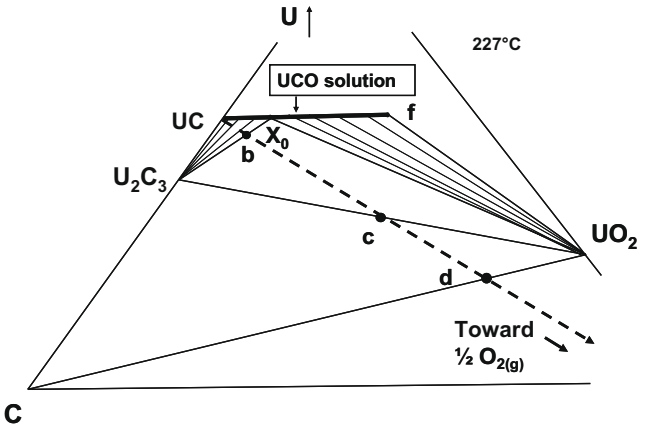

Fig. 2. Isothermal calculated cross-section at 227 °C of the U-C-O ternary phase diagram. The dashed line corresponds to the equilibrium oxidation path from UC to UO_2 at 227 °C and 1 bar.

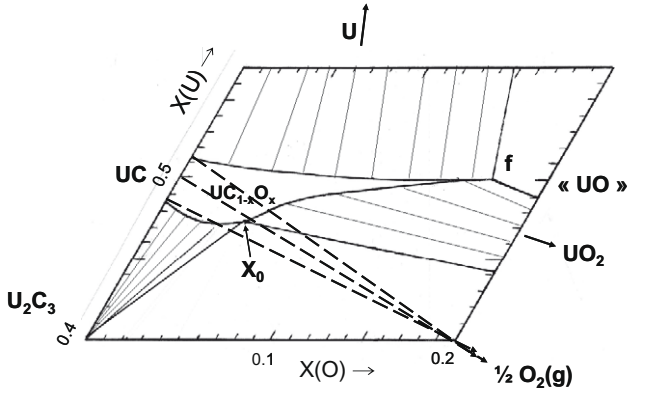

Fig. 3. Detail of the phase diagram around the monophasic solid solution $UC_{1-x}O_x$ as calculated at near room temperature. Three different oxidation paths are presented starting from different U/C initial ratios in the non-stoichiometric UC compound.

and with a composition domain quite similar to the one determined at high temperature. The limits of the solid solution have been measured only in the 1300–1700 °C temperature range and the different authors did not observe significant changes as stated by Guéneau in the optimization process. This feature can be related either to the compound itself in the analyzed temperature range or to the quenching process due to low diffusion rate of the components. Fig. 3 shows a detail of the isothermal cross-section at 227 °C with special points b–d along the UC oxidation path, i.e. corresponding to overall compositions at equilibrium when UC reacts with oxygen at equilibrium. The point f corresponds to the UCO_{sat} composition, where the $UC_{1-x}O_x$ solid solution composition reaches its maximum oxygen content ($UC_{0.65}O_{0.35}$ at $T = 227$ °C).

The UC ignition phenomenon basically consists in the overall reaction $UC(s) + O_2(g) \rightarrow (s) + CO(g)$ that produces considerable heat of reaction (1098 kJ/mol at 25 °C) and may cause a considerable temperature increase. The ignition path should be analyzed as an oxidation which takes into account the temperature and mass balance at any time. It is a summation of different events occurring in relation with the phase diagram. Consider the following series of equilibrium states:

- At the beginning of the oxidation reaction, the UC is transformed in a $UC_{1-x}O_x$ solid solution up to the composition $\mathbf{X_0}$, i.e. $UC_{0.95}O_{0.05}$ by oxygen diffusion in conjunction with the creation of the U_2C_3 phase in equilibrium till **b** total composition.
- Between **b** and **c** compositions, a third condensed phase C appears, in the triphasic $UC_{0.95}O_{0.05}$–U_2C_3–C domain.
- Between **c** and **d** compositions, the UO_2 phase appears in presence of carbon. At that time, normally the thermal effect should increase rapidly depending on the UO_2 amount formed per second.
- When the amount of oxygen leads to point **d** which corresponds to the two-phase UO_{2-x}–C domain, the gaseous pressure increases continuously according to the phase rule (variance is equal to 1). At one point labeled **e** (see Fig. 4) the gas phase, composed mainly by CO(g) and CO_2(g), will reach 1 bar total pressure.

The non-stoichiometry of UC has also to be considered, as shown in Fig. 3 which is a zoom of the ternary phase diagram in the UC region. Note that the proposed diagram by Henry et al. [17] at high temperature is quite different from the one calculated near room temperature since the solution UCO could be in equilibrium with UC_2 or C.

In Fig. 3, we observe also that the formed phases for oxidation at equilibrium may depend on the initial U/C composition ratio: (i) a U rich carbide will favor the direct formation of a UO_2 surface layer and (ii) a C rich carbide will precipitate primarily carbides (or carbon according to Henry et al. [17] at the surface before forming a UO_2 layer.

The gas pressure due to the oxidation reaction can be calculated in two ways:

- The first way consists in calculating the pressure along the UC–½O_2(g) overall composition path to identify the composition point when the pressure can become high enough to prevent the incoming oxygen to reach the UC surface or to create a blast effect.
- The second way consists in specifying a given triphasic composition (variance is equal to 0 for a given temperature and pressure is fixed) and make the temperature varying; this procedure allows us to estimate the temperature at which the pressure of the reaction products reaches the total pressure applied to the system, generally atmospheric pressure: we assume that ignition occurs at an instantaneous overall composition in the same triphasic mixture.

We calculated the pressure along the UC-½O_2 path for various temperatures, assuming an isothermal system. This allowed us to identify the overall reaction product composition at which the equilibrium pressure increases spontaneously with regards to the chemical composition of the system (flame temperature is not here calculated from adiabatic conditions). Fig. 4 shows for example the calculated CO(g) pressure at 1300 °C along the reversible oxidation composition path: for compositions lower than $x(O) = 0.5$, the CO(g) pressure remains low and constant (10^{-5} bar). It abruptly increases for a molar oxygen fraction of 0.5. This sudden increase could result in a blast effect or a detonation in the sample as long as oxygen is provided to the sample. In this plot calculated at a given temperature, it is possible to follow the path from a two-phase domain (UCO + U_2C_3 or C–UO_2) where pressure varies to three-phases domains where pressure is fixed.

Due to low equilibrium oxygen pressures till $x(O) = 0.5$, the CO_2(g) pressure remains lower than the CO(g) pressure. Then, due to the high temperature chosen here, CO(g) remains more important, except when going to UO_{2+x} hyperstoichiometric uranium oxide.

To follow experimentally the oxidation path proposed in the ternary phase diagram, as well as to explore the possibility of other paths due to some kinetic limitations, analysis of the phases present either after complete oxidation, or after stopping the oxidation when a particular event is observed by DTA/TGA has been included in the experimental procedure.

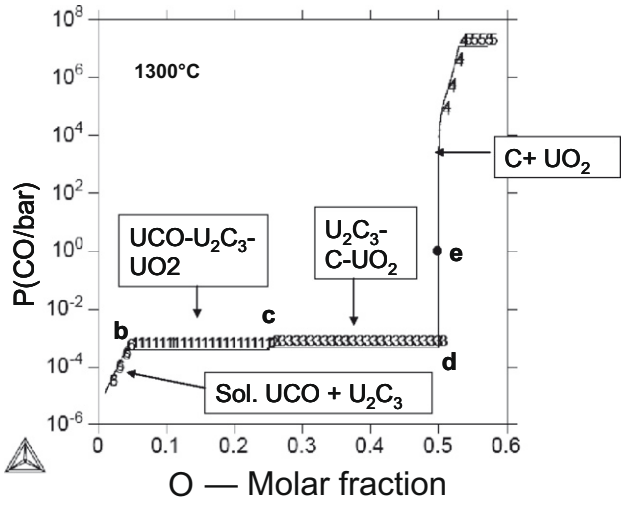

Fig. 4. Calculated equilibrium CO pressure (bar) at 1300 °C along the UC–½O_2(g) path.

4. Experimental

Differential thermal analysis (DTA) and thermogravimetric analysis (TGA) were performed and combined with characterizations of the samples by X-ray diffraction (XRD).

A preliminary standard test was carried out with UC powders (milled during 5 h), a heating rate of 5 °C min^{-1} under a dry air flow rate of 2 l/h. Three exothermic peaks were observed on the DTA curve for this test in Fig. 5. A first reaction is visible at a temperature of 140 °C, and a major exothermic phenomenon is observed near 200 °C corresponding to ignition. In the following runs, the partially oxidized powders were analyzed by XRD (Fig. 6) when stopping the temperature ramp after each thermal accident, inerting in pure 6.0 Ar and cooling down to room

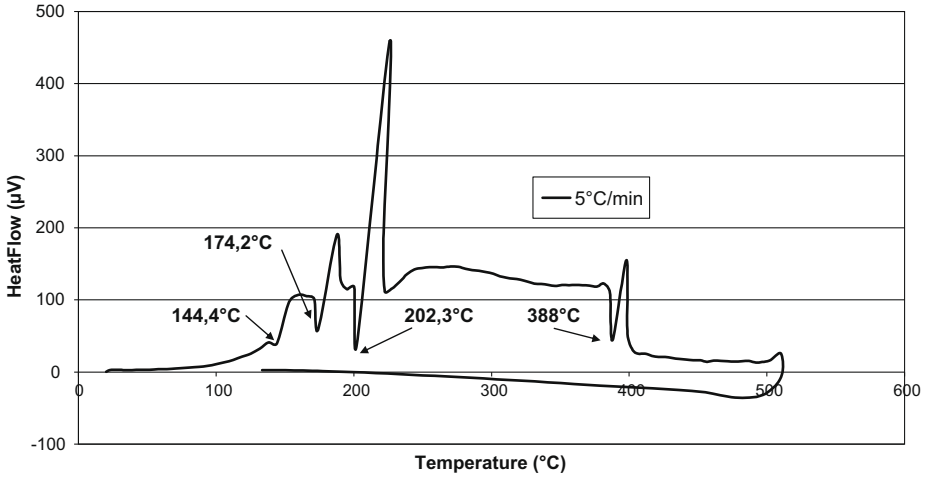

Fig. 5. DTA for the standard test at 5 °C min^{-1} up to 500 °C under dry air (2 l/h) and cooling down under pure Ar 6.0.

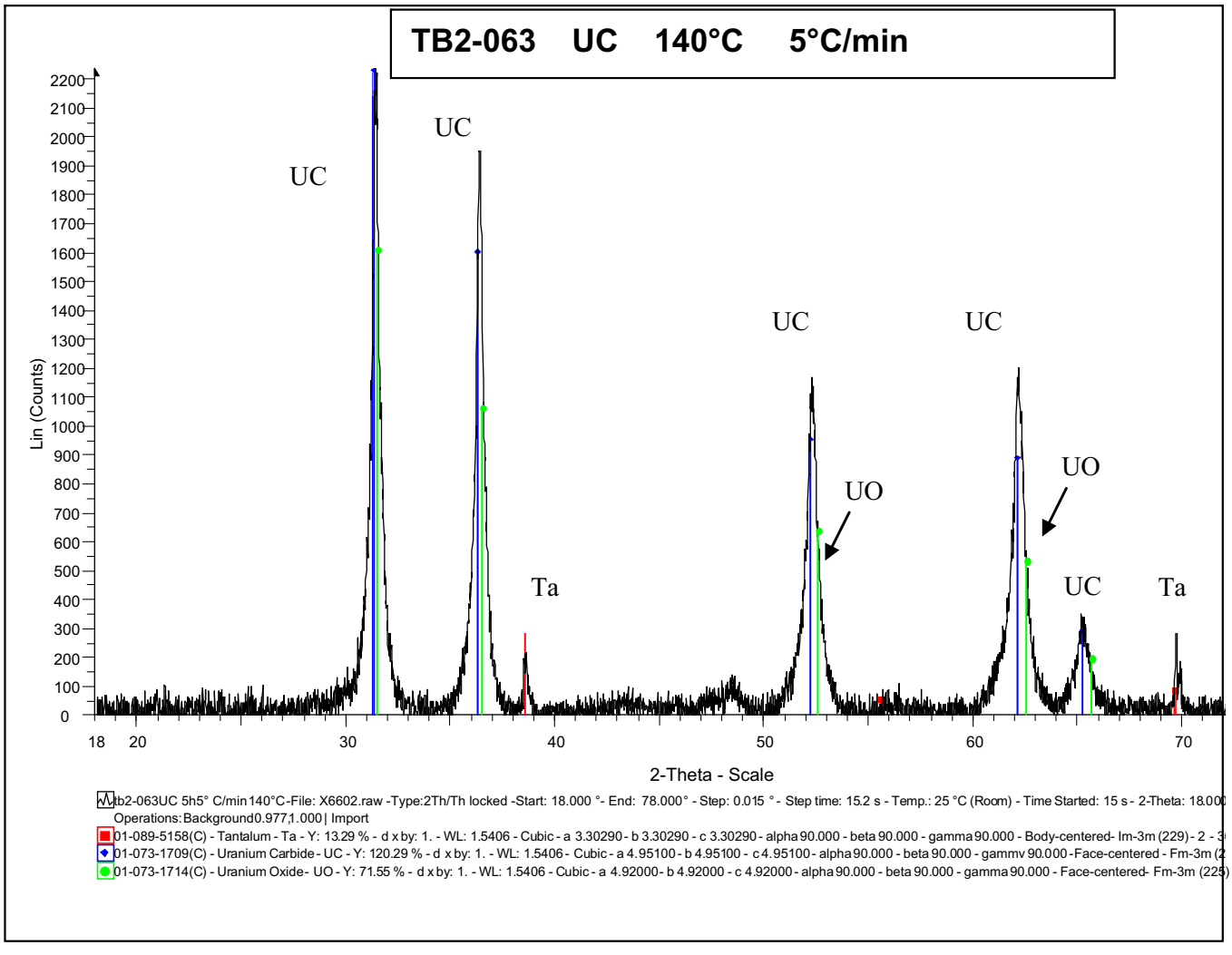

Fig. 6. XRD pattern after DTA in flowing air on UC milled during 5 h, heating rate 5 °C min^{-1}, oxidation test stopped at 140 °C and cooling in pure argon.

temperature with a 20 °C min^{-1} ramp. The phases identified after each shutdown are indicated in Table 2.

Fig. 7 gives the experimental lattice parameters for the UCO solid solution as reported in literature. Comparison between these data and the obtained XRD information (Table 3) obtained from XRD pattern (Fig. 8) suggest that oxygen diffusion has occurred in the UC compound at 140 °C (smaller lattice parameter) to reach the UCO_{sat} solid solution (**f** composition in Fig. 2).

Table 2
Characterization of the phases obtained when stopping the standard oxidation tests after each thermal effect. UCO_{sat} represents the oxygen-saturated UCO solid solution (point **f** in Error! Reference source not found).

Shutdown temperature (°C)	140 °C	200 °C	275 °C	330 °C	500 °C
Post experimental XRD phases identification	UCO_{sat}	UC major phase + UO_2	UC + UO_2 major phase	UO_2	U_3O_8

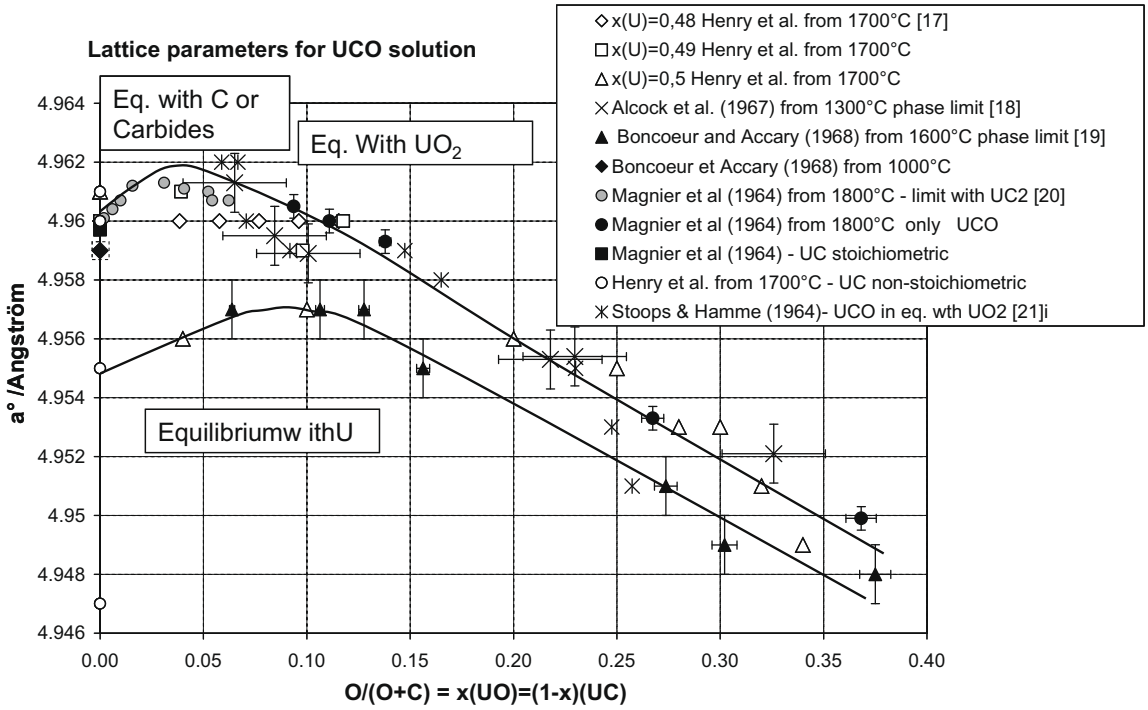

Fig. 7. Summary of lattice parameters as measured for the solid solution $UC_{1-x}O_x$ either in equilibrium with C or Uranium. It is not possible to distinguish between pure UC from the solution for x=0.1 with the only lattice parameter determination. (See above mentioned References for further information.)

Table 3
Calculated UC lattice parameter (cubic lattice) for the standard test from XRD spectra.

	UC ref	140 °C	200 °C	275 °C
a (max obs) in Å	4.955	4.948	4.957	4.958

That feature seems not compatible with the equilibrium oxidation expected from the phase diagram that predicts the composition at $\mathbf{X_0}$ i.e. close to pure UC ($UC_{0.95}O_{0.05}$) in equilibrium with U_2C_3.

Note that the smaller lattice parameter observed could also correspond to stress in the underlying UC, due to compression by an external layer, but the great difference in the lattice parameters let this assumption to be the less probable.

Above 140 °C the calculated UC lattice parameters remain close to its initial value that is for compositions between UC and UCO at $\mathbf{X_0}$ ($UC_{0.95}O_{0.05}$); the UCO saturated solid solution apparently disappeared or could be present only as a very thin and not detectable intermediate layer. Note that according to phase diagram the UCO(sat) composition at **f** cannot be in equilibrium (local equilibrium) with UO_{2+x} *compound* i.e. oxygen enriched by oxidation. The only situation allowing UCO(sat) to exist would be low oxygen diffusion in a compact and protecting UO_2 layer preventing oxygen to reach directly the carbide phase.

The broad and centered UO_2 peaks indicate that the UO_2 was partly uncrystallized or present in the form of small grains. For each temperature, lattice parameter is an average value of *a* (Å) obtained from the four main (1 1 1), (2 0 0), (2 2 0) and (3 1 1) UC peaks. Lattice parameter *a* (Å) values have been revalued since [4] and are given with an accuracy of 0.02%.

XRD pattern as shown in figure XRD 1 was submitted to Debye–Scherrer method for lattice parameter calculation. In the UC cubic lattice, d(h,k,l) value for each (h,k,l) peak is depending only on the lattice parameter *a* (Å). XRD software calculates d(h,k,l) value for each (h,k,l) peak using Bragg law. Lattice parameter *a* (Å) value is calculated from following relation:

$$a = d_{hkl}\sqrt{h^2 + k^2 + l^2}.$$

Rietveld measurement will be performed in the future on several XRD pattern to complete the study.

The observation of the saturated solid solution at 140 °C confirms the calculated phase diagram (Fig. 1) and the existence of the solid solution at low temperature.

The effect of the particle size fractions, the heating rate, and the oxygen concentration in the atmosphere have been also investigated. The influence of the heating rate and oxygen concentrations will be discussed in this article. The DTA curves obtained for heating rates of 3, 5 and 10 °C min^{-1} are compared in Figs. 9 and 10.

The 3 °C/min test showed the same type of DTA peaks as the 5 °C/min test. The spontaneous exothermic phenomenon at 230 °C (ignition) in the 3 °C min^{-1} test resulted in part of the sample ejection from the crucible as observed in the TGA curve monitored simultaneously, which was attributed to sudden gas release in relation with a rather important mass and probably more important temperature increase. XRD analysis of the sample oxidized at 500 °C revealed a single U_3O_8 phase (see Figs. 11 and 12).

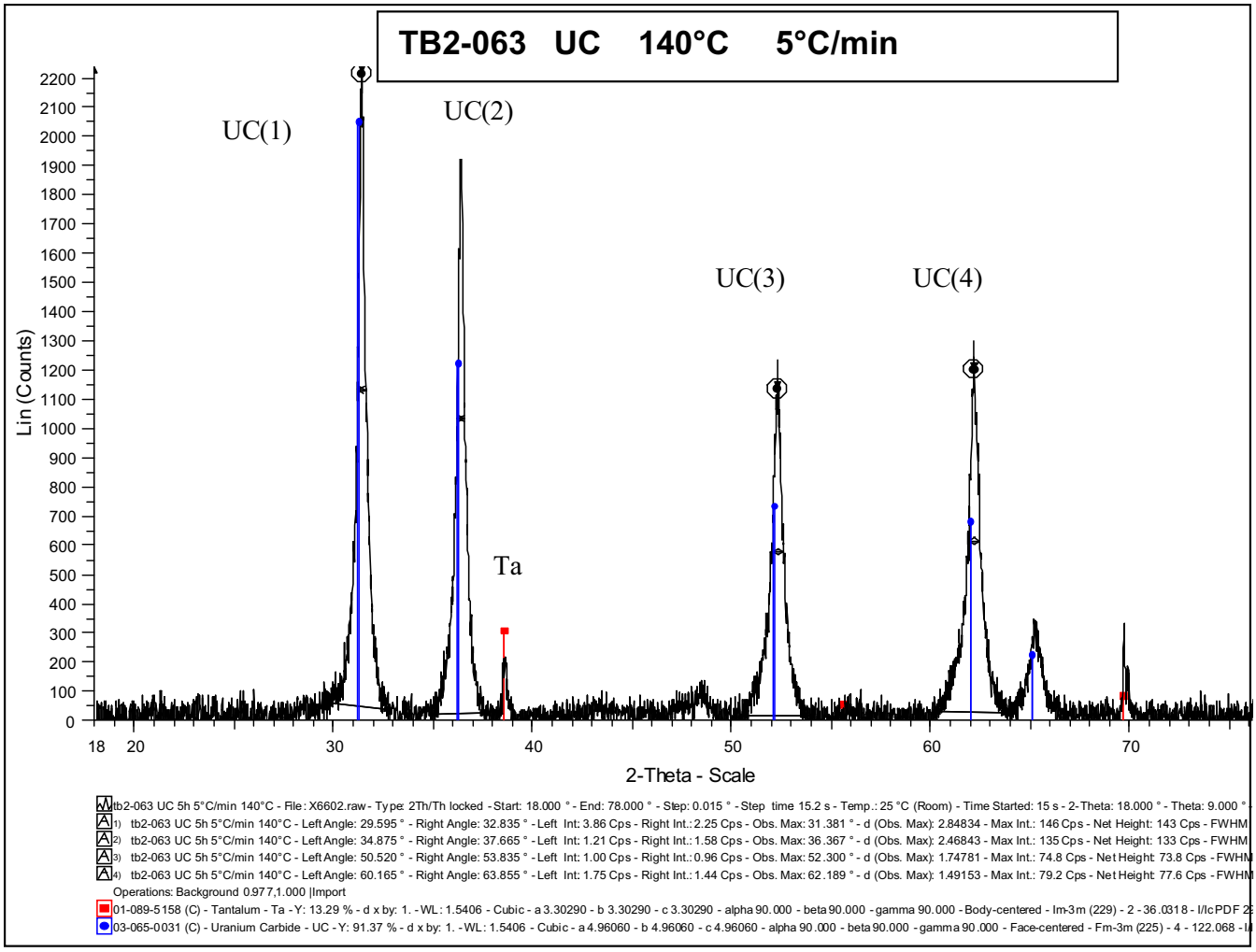

Fig. 8. XRD pattern and lattice parameter identification on the four main peaks of UC cubic lattice after DTA in flowing air on UC milled during 5 h, heating rate 5 °C min^{-1}, oxidation test stopped at 140 °C and cooling in pure argon (calculations from XRD pattern in Fig. 6).

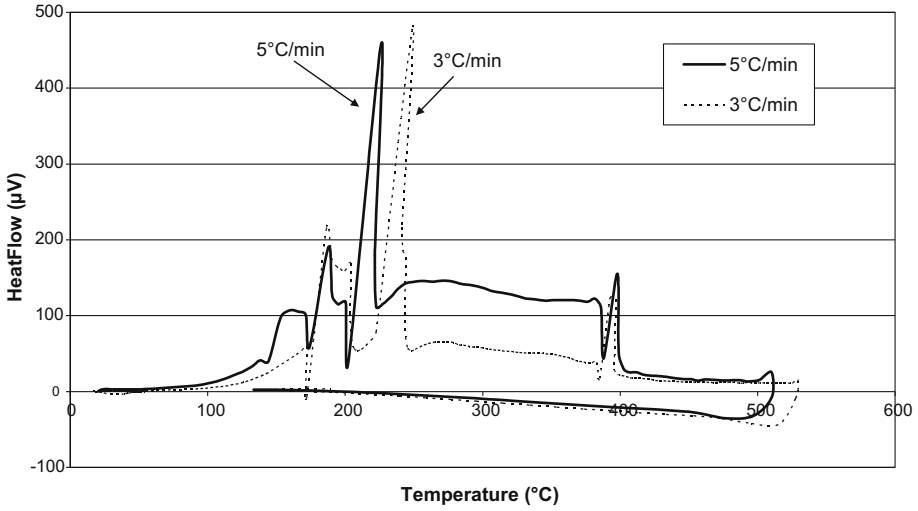

Fig. 9. Effect of heating rate in DTA on oxidation of UC under dry air (2 l/h): rate 3 °C min^{-1} (broken line), rate 5 °C min^{-1} (full line).

No DTA peak was observed for the 10 °C/min test. Powder samples oxidized at 10 °C min^{-1} were analyzed by XRD after stopping the temperature ramp at 140 and 200 °C, inerting in Ar 6.0, and cooling. The phases present after each shutdown are indicated in Table 4.

Unlike the standard test at 5 °C min^{-1}, the UC peaks were well centered and narrow and the calculated UC lattice parameter suggests a very small dissolution of oxygen in the UC (Table 5). Note, in agreement with the DRX results in Fig. 6, that the lattice param-

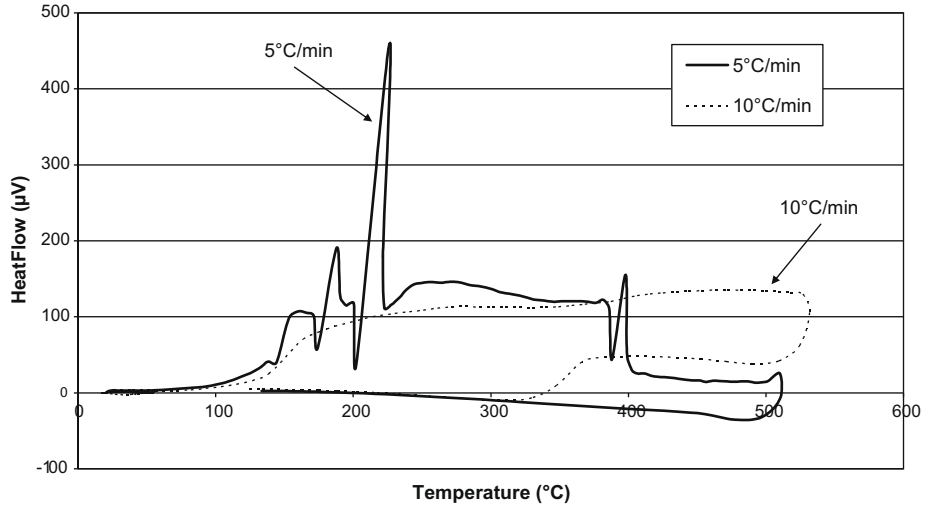

Fig. 10. Effect of heating rate in DTA on oxidation of UC under dry air (2 l/h): rate 10 °C min^{-1} (broken line), rate 5 °C min^{-1} (full line).

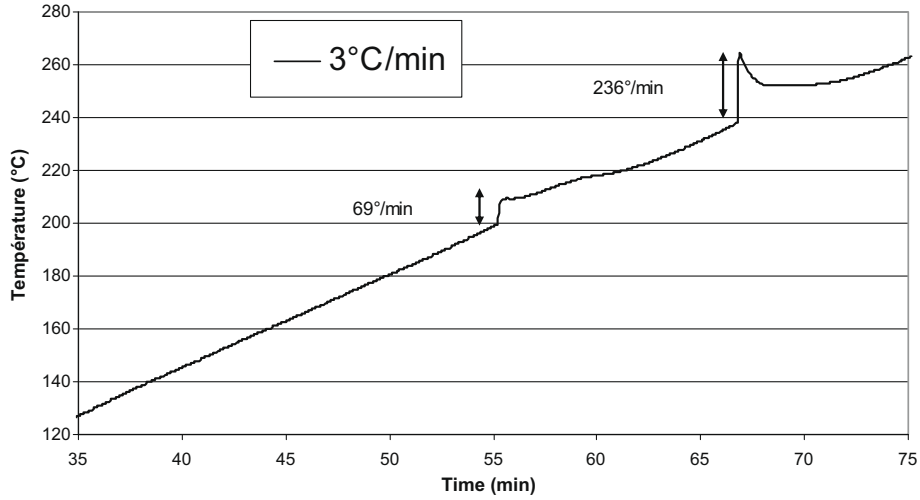

Fig. 11. Temperature measured beneath the sample crucible for an oxidation test (3 °C min^{-1}) in air (2 l/h) with UC milled during 5 h.

eter for low oxygen compositions ranges in the same limits that the non-stoichiometric one for $UC_{1\pm x}$.

The UO_2 peaks were narrow and shifted to the left. UO_2 appeared to be better crystallized than in the standard test and the shift could correspond to tensile loading.

When testing the effect of O_2 concentrations in the flowing gas, two trends were observed: for less than 5% O_2 in Ar, the sample oxidizes as for heating rates of 10 °C min^{-1} in air without ignition, whereas above 5% O_2 in Ar, the sample ignited and the DTA spectra were identical to those of the standard test.

5. Interpretation and discussion

Musgrave [22] developed a model of ignition of uranium-bearing products, and defined the pyrophoricity as the point when the material temperature rise is above 100 °C min^{-1}. In our tests the temperature beneath the sample crucible was continuously monitored and the exothermic peaks on the DTA curves correspond to a sudden temperature rise. For example, a temperature rise of 236 °C min^{-1} has been observed during the test at 3 °C/min ramp. It was associated with sample release from the crucible for the main DTA peak.

Calculations as displayed in Fig. 4 show that the sudden CO(g) pressure rise is observed only in the two-phases UO_{2-x}–C zone, which occurs at point **d**, in terms of the overall system composition—since all the uranium bound to carbon in UC would then have to be consumed as UO_{2-x}. However, such situation could concern only an external "active" layer of the samples since the heat produced at least at the first peak does not concern the entire UC bulk sample. Different critical oxidized layers thickness could be involved and the ignition process could be reproduced as cycles by successive destruction of these layers: this effect is expected to be related either to the only material layered structure during ignition or to the depletion of oxygen flux at the surface of the powder in the cylindrical crucibles when ignition starts.

The overall composition for oxidation will be unlikely to be maintained along the C–UO_2 line at point **e** (Fig. 4) for which the high CO and CO_2 pressure will result in carbon loss, modifying the overall UC–UO_2 composition and deviating from the UC–½O_2(g) line toward UCO solutions and UO_2. If the combustion reaction continues it will not only consume the residual C, producing CO(g), but also produce higher oxides such as U_4O_9, U_3O_8 or even UO_3.

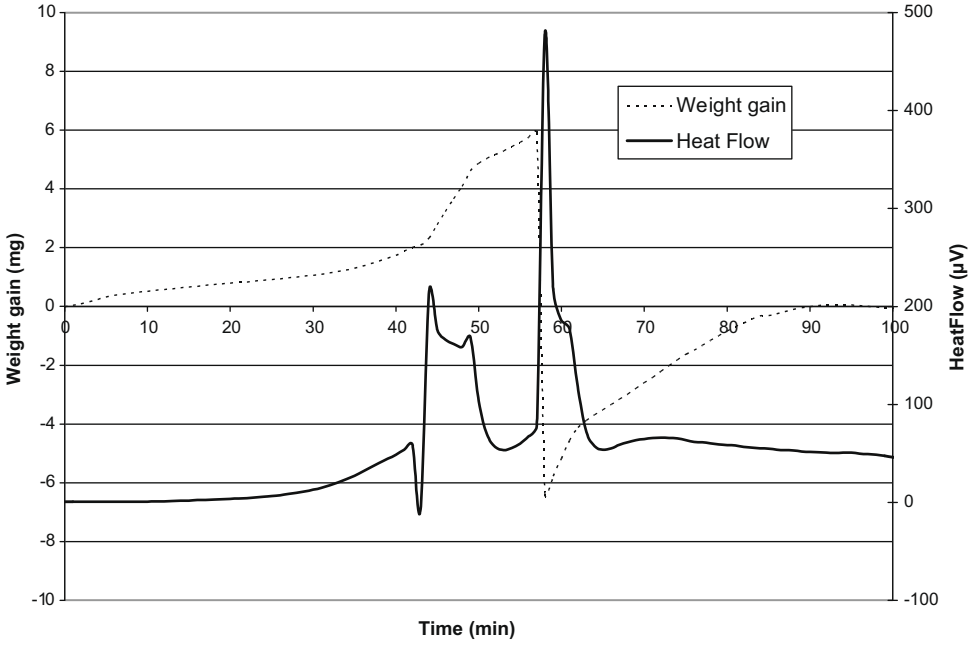

Fig. 12. Violent ejection of sample from crucible during an oxidation test (3 °C min^{-1}) in air (2 l/h) with UC milled during 5 h: mass variation (broken line), heatflow DTA (full line).

Table 4
Characterization of the phases present at different stages for the 10 °C min^{-1} oxidation tests.

Shutdown temperature (°C)	140 °C	200 °C	500 °C
Post experimental XRD phases identification	UC	UC UO_2	U_3O_8

Table 5
Calculated UC lattice parameter (cubic lattice) after the 10 °C min^{-1} test.

Shutdown temperature	UC ref	140 °C	200 °C
a (max obs) in Å	4.955	4.960	4.962

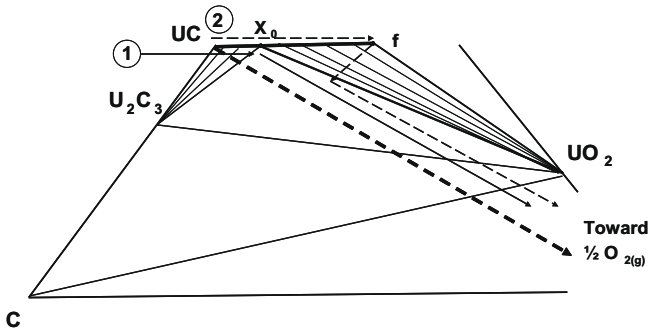

Fig. 13. Two hypothetical and possible UC oxidation paths (named 1 and 2) based on the U–C–O diagram calculated at 227 °C and on our experimental observations.

At the beginning of the oxidation process, due to layer(s) growth kinetics and mainly oxygen diffusion to create UCO solutions, the path followed for the overall composition balance of the "active" layer may not be the UC–½O_2(g) composition line but based mainly on the $UC_{1-x}O_x$ phase limit. Indeed, from the lack of XRD observation of U_2C_3 or UC_2 and free C in elemental chemical analysis of the samples, and assuming the UCO solution is present systematically when UC is in contact with an oxidizing atmosphere, due to a necessary oxygen chemical potential gradient at the interface, two oxidation paths are therefore possible according to our observations and U-C-O phase diagram (Fig. 13).

A first path based on the UCO phase limit then on UCO–UO_2 equilibrium: this path shown as 1 in Fig. 13 could correspond either to rapid heating rates in air (10 °C min^{-1} or 20 °C min^{-1}) or to low oxygen concentrations in argon (1% and 3% O_2), that is respectively either not enough time for oxygen diffusion or not enough available oxygen content to build up a thick UCO_{sat} layer. XRD analysis of the oxidation product at 200 °C revealed the presence of quasi-pure UC and a well crystallized UO_2 showing:

- the formation of a UO_2 layer and oxygen diffusion controlled through this layer, generating a regular thermal contribution,
- regular heat exchange by thermal diffusion from the UC core to its environment,

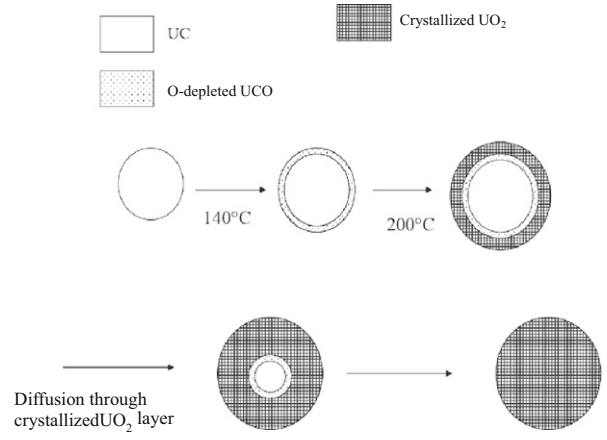

Fig. 14. Proposed UC oxidation mechanism following the path 1: stable double layer UCO/UO_2.

- satisfactory mechanical contact and stable adherence of UO_2 to the necessary underlying UCO layer with low oxygen content. This intermediate layer is necessarily thin (no XRD detection) and not oxygen-saturated (point $\mathbf{X_0}$ or quasi-equilibrium conditions with UO_{2-x}).

These assumptions could account for the continuous heat release observed by DTA, very near the standard test but without any thermal accident. In this case the mechanism (Fig. 14) would be a diffusion reaction from the beginning to the end of oxidation with a stable double layer UC(O)/UO_{2-x} even if the external oxide finally becomes a brittle U_3O_8 oxide as observed at the end of the experiment.

A second path based on the appearance of the UCO phase saturated with oxygen (path 2 in Fig. 13). This situation is attained if oxygen diffusion predominates over nucleation/precipitation of UO_2 at least in a first step: oxygen would enrich the UC surface with a layer of $UC_{1-x}O_x$ until saturation (point **f**). Due to the single-phase nature of the solution and its capability to match as a function of the oxygen content between the lattice of UC and at the lattice of UCO_{sat}, the nucleation of UO_2 is easier and a layer of UO_{2-x} would form. The lattice mismatches being more compatible, the UCO solution could be mechanically stable for a longer time and could also be thicker. This path would involve slow heating rates leading to the slow and reversible formation of a thick and compact layer of UCO solid solution around a UC core prior to the formation of UO_2 on the surface.

Ignition would occur with the sudden rupture of this double layer –mechanical failure of the double layer probably due to the constraint of the UO_2 external layer which increases with thickness – and oxygen suddenly gained access to the residual internal UC. The surface of UC would react to form a new UCO layer on which new compact UO_2 could form again until reaching a critical thickness and rupturing once again. This cyclic phenomenon would correspond to the different exothermic peaks observed by DTA. After two or three ignitions, the structure becomes fractured and the UO_2 phase forms at the same rate as the UCO phase; this accounts for the absence of any additional sudden exothermic phenomena detrimental to continuous oxidation till the final oxidation into U_3O_8 corresponding to the last thermal effect at about 400 °C.

The process thus basically consists in an oxygen diffusion mechanism through a compact UO_2 layer and an interfacial reaction mechanism when this layer breaks down. Based on different DTA findings the two conditions: (i) low heating rates of 3 or 5 °C/min under air or (ii) oxygen concentration exceeding 5% at a flow rate of 2 l/h, correspond to slow access of oxygen to the UC surface and oxygen diffusion becoming predominant. At temperatures up to 140 °C (point 1 in Fig. 5), the UC lattice parameter is observed to decrease (from 4.955 Å initially to 4.948 Å at 140 °C) and the UC XRD peaks shift toward a higher angular range corresponding to the presence of oxygen in the UC. The value of the lattice parameter at 140 °C suggests that the oxygen solubility limit of about 37 mol% has been reached in the UC. Since at this temperature the UO_2 phase has not yet appeared, this would be the limit of the UCO equilibrium line in the phase diagram at 140 °C, confirming the low temperature extrapolation performed in the phase diagram calculations. We remind that solubility limits of the UCO solutions were determined as quite constant in the 1300–2300 °C temperature range [12].

At 200 °C (point 2 in Fig. 5) the UC lattice parameter returns to its initial value – which is in fact UC or more probably $UC_{0.95}O_{0.05}$ – and the UO_2 phase appears (as enlarged XRD peaks). Based on the path 2 in Fig. 13 it can be assumed that the formation of UO_2 consumes suddenly the thick UCO layer produced earlier. The shape of the UO_2 peaks is characteristic of small, relatively uncrystallized UO_2 grains forming a thermal and oxygen diffusion barrier layer. This hypothetical oxidation mechanism is shown schematically in Fig. 15.

6. Prospects

The proposed mechanisms are based on both thermodynamic assumptions and observations of DTA experiments together with XRD phase analysis. Two types of experiments are now in progress to validate this hypothesis:

1. Monitoring the oxidation kinetics of oxidized solid uranium carbide beads at specified temperatures by SEM and EDS analysis on polished cross-sections should allow us to observe changes in conditions and grain morphology variations related to the different oxidation steps.
2. The set up of a mass spectrometer with capillary sampling on DTA should allow us to observe the nature and pressure of the gases released during oxidation in order to correlate the ignition phenomenon to the observed DTA peaks, mass variations and resulting phases.

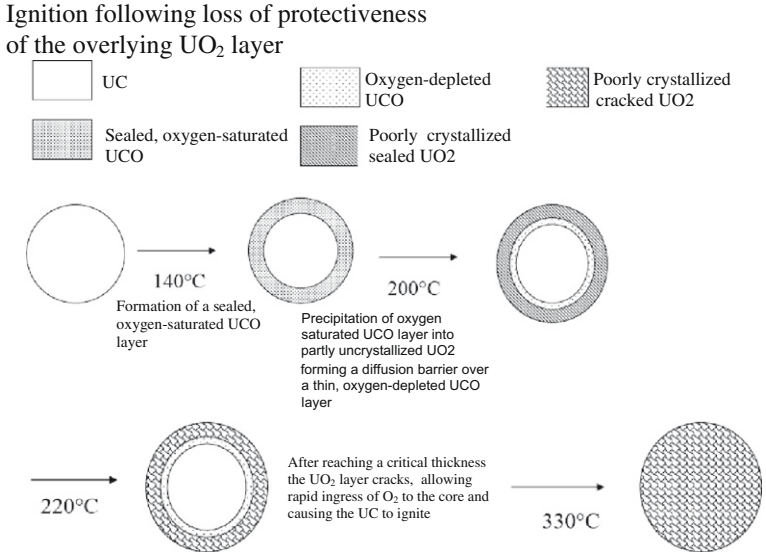

Fig. 15. UC oxidation mechanism following path 2 in Fig. 10 and leading to ignition.

7. Conclusions

The present experimental DTA study identified variations in the oxidation behavior of uranium monocarbide powder samples related to various parameters such as the reached temperature, the heating rates, and the atmospheric oxygen concentration. Exothermic phenomena (DTA peaks) indicated ignition temperatures of about 200 °C, an extremely violent phenomenon observed in air flow rate of 2 l/h and at heating rates of 3–5 °C min^{-1}.

Conditions for ignition limitations were observed. X-ray diffraction analysis of powder samples after the oxidation test established a relationship between the phases formed and the thermal cycle. Combined with thermodynamic calculations in the U-C-O ternary phase diagram, these considerations make it possible to construct oxidation pathways and to propose possible mechanisms.

These mechanisms are based on the nature of the oxide layers or bi-layers formed (UCO solid solution and UO_2 oxide) and on the sudden or progressive fracture of these layers. These assumptions must still be validated by further investigations using mass spectrometry in order to determine the nature and pressure of the gases released by oxidation ramps and observation of the oxide layers on polished cross-sections to complete isothermal kinetic studies on solid UC samples. It is of first importance to understand the oxidation mechanisms since despite the low test temperatures, the thermodynamic simulation based on the interpretation of experimental observations and the CO gas release primarily during ignition suggest that temperatures far above 1500 °C could be reached during powder ignition, accompanied with a blast effect.

Furthermore, in addition to these material considerations, simulations of the thermal aspects of UC ignition using heat and mass transfer analysis are going on.

References

[1] P. Martin, N. Chauvin, J.C. Garnier, M. Masson, P. Brossard, P. Anzieu, in: Proceedings of GLOBAL 2005, Tsukuba, Japan, 9–13 October 2005.
[2] V.J. Wheeler, R.M. Dell, AERE R-4600 (1964).
[3] S.M. Mukerjee, G.A. Rama Rao, J.V. Dehadraya, V.N. Vaidya, V. Venugopa, J. Nucl. Mater. 210 (1994) 97.
[4] F. Le Guyadec, S. Joffre, C. Chatillon, E. Blanquet, in: Matériaux 2006, Dijon, France, 13–17 November 2006.
[5] R. Sowden, N. Hodge, in: Proceedings Symposium Carbides in Nuclear Energy, Harwell, November 1964, p. 297.
[6] E.W. Murbach, Metallurg. Petrol. Eng. 227 (1963) 488.
[7] C. Guéneau, S. Chatain, S. Gossé, C. Rado, O. Rapaud, J. Lechelle, J.C. Dumas, C. Chatillon, J. Nucl. Mater. 344 (2005) 191.
[8] S. Gossé, C. Guéneau, S. Chatain, C. Chatillon, J. Nucl. Mater. 352 (2006) 13.
[9] C. Guéneau, S. Chatain, J.C. Dumas, J. Lechelle, C. Rado, F. Defoort, N. Dupin, B. Sundman, H. Noel, R. Konings, in: Third International Topical Meeting on High Temperature Reactor Technology, Johannesburg, South Africa, 1–4 October 2006.
[10] P.Y. Chevalier, E. Fischer, J. Nucl. Mater. 288 (2001) 100.
[11] C. Guéneau, M. Baïchi, D. Labroche, C. Chatillon, B. Sundman, J. Nucl. Mater. 304 (2002) 161.
[12] D. Labroche, O. Dugne, C. Chatillon, J. Nucl. Mater. 312 (2003) 21.
[13] D. Labroche, O. Dugne, C. Chatillon, J. Nucl. Mater. 312 (2003) 50.
[14] M. Baïchi, C. Chatillon, G. Ducros, K. Froment, J. Nucl. Mater. 349 (2006) 57.
[15] M. Baïchi, C. Chatillon, G. Ducros, K. Froment, J. Nucl. Mater. 349 (2006) 17.
[16] T. Bessmann, J. Am. Ceram. Soc. 66 (1983) 353.
[17] J.L. Henry, D.L. Paulson, R. Blickensderfer, H.J. Kelly, Report of Investigations 6968, Bureau of Mines, 1967.
[18] C.B. Alcock, N.A. Javed, B.C.H. Steele, Bull. Soc. Franç. Céram. 77 (1967) 99.
[19] M. Boncoeur, A. Accary, J. Nucl. Mater. 25 (1968) 271.
[20] P. Magnier, J. Trouvé, A. Accary, Carbides in Nuclear Energy, vol. I, Macmillan, London, 1964. p. 95.
[21] R.F. Stoops, J.V. Hamme, J. Am. Ceram. Soc. 47 (1964) 59.
[22] L. Musgrave, J. Nucl. Mater. 42 (2) (1972).